Nonlinear energy response of glass forming materials

2008 J. Phys.: Condens. Matter 20 035105

(http://iopscience.iop.org/0953-8984/20/3/035105)

IOP PUBLISHING JOURNAL OF PHYSICS: CONDENSED MATTER

J. Phys.: Condens. Matter **20** (2008) 035105 (9pp) doi:10.1088/0953-8984/20/03/035105

Nonlinear energy response of glass forming materials

Fumitaka Tagawa[1] **and Takashi Odagaki**

Department of Physics, Kyushu University, Fukuoka 812-8581, Japan

E-mail: F_tagawa@si-seiko.com

Received 1 September 2007, in final form 13 October 2007
Published 17 December 2007
Online at stacks.iop.org/JPhysCM/20/035105

Abstract

A theory for the nonlinear energy response of a system subjected to a heat bath is developed when the temperature of the heat bath is modulated sinusoidally. The theory is applied to a model glass forming system, where the landscape is assumed to have 20 basins and transition rates between basins obey a power law distribution. It is shown that the statistics of eigenvalues of the transition rate matrix, the glass transition temperature T_g, the Vogel–Fulcher temperature T_0 and the crossover temperature T_x can be determined from the first- and second-order ac specific heats, which are defined as coefficients of the first- and second-order energy responses. The imaginary part of the first-order ac specific heat has a broad peak corresponding to the distribution of the eigenvalues. When the temperature is decreased below T_g, the frequency of the peak decreases and the width increases. Furthermore, the statistics of eigenvalues can be obtained from the frequency dependence of the first-order ac specific heat. The second-order ac specific heat shows extrema as a function of the frequency. The extrema diverge at the Vogel–Fulcher temperature T_0. The temperature dependence of the extrema changes significantly near T_g and some extrema vanish near T_x.

1. Introduction

Since the anomaly of the specific heat at the glass transition was discovered in 1923 [1], many studies have been conducted to understand the behavior. Since the anomaly depends on the measurement process, the transition is now believed not to be understood in the framework of the standard thermodynamics [2].

Recently the concept of the landscape has been paid much attention because of the possibility to explain the transition in non-equilibrium systems [3, 4]. In particular, the free energy landscape (FEL) picture proposed by Odagaki *et al* [5, 6] is considered to provide the unified concept for understanding thermodynamic and dynamic singularities of the glass transition. In fact, the single-particle dynamics [7] and the specific heat [8–14] were shown to be phenomenologically well described by the framework based on the FEL. Namely, the dynamical transition is understood as the Gaussian-to-non-Gaussian transition [7], and the thermodynamic singularities near T_g, including the cooling rate dependence of the specific heat, are characterized as the quenched-to-annealed transition in dynamics on the FEL [8–11].

[1] Present address: Seiko Co., Ltd, Fukuoka, Japan.

The specific heat of non-equilibrium systems such as glass forming materials is defined by the response of the energy to a unit rise of temperature [15]. Because of the slow relaxations, the system cannot reach equilibrium during the measurement and the energy response shows a time delay. Therefore one can expect that the ac specific heat [16, 17] will contain information on the slow dynamics. The ac specific heat $\tilde{C}_1(\mathrm{i}\omega)$ is defined as the Laplace–Fourier transform of the energy or enthalpy correlation function $\phi(t)$ [14, 18].

$$\tilde{C}_1(\mathrm{i}\omega) = \int_0^\infty \mathrm{d}t\phi(t)\mathrm{e}^{-\mathrm{i}\omega t}. \tag{1}$$

The ac specific heat is often fitted by the Laplace–Fourier transform of the stretched exponential $\phi(t) = \exp(-(t/\tau)^\beta)$, since the correlation function is believed to be the superposition of the Debye relaxation function with different relaxation times. However, the origin of the distribution of the relaxation times has not clearly been understood.

So far, studies of the energy response of glass forming systems have been limited within the linear response region, and the nonlinear energy response has not been studied yet. In a previous paper [14], we proposed the description of the

first- and second-order energy response with the free energy landscape picture and applied it to a two-level system with a diverging barrier. It is shown that the second-order energy response has a diverging term at the temperature where the relaxation time diverges.

In this paper, we investigate the linear and nonlinear energy responses of non-equilibrium systems described by the FEL picture to an oscillating temperature and present the characteristic behavior of the first- and second-order ac specific heat. Using a model FEL which supports a glass transition, we show that the Vogel–Fulcher temperature and the crossover temperature as well as the glass transition temperature can be determined from the characteristic behavior of the ac specific heats. We also show that the statistics of the transition rate matrix representing the stochastic dynamics among the basins of the FEL can be obtained from the frequency dependence of the first-order ac specific heat. In addition, the divergence of the second-order ac specific heat is observed at the Vogel–Fulcher temperature. This behavior is similar to the divergence of the nonlinear susceptibility of the spin glass system and is first measured in the glass forming model.

The organization of the paper is as follows. In section 2, we explain the first- and second-order energy responses when the temperature of the heat bath is oscillated sinusoidally. The definition of the first- and second-order ac specific heat is also given. In section 3, the stochastic dynamics on the free energy landscape is explained. In section 4, we describe the first- and second-order energy responses to the oscillating temperature and the first- and second-order ac specific heats when the system is described by the FEL picture. As an example, a model system with FEL consisting of 20 basins is analyzed. In section 5, where transition rates between basins are assumed to obey a power law distribution, we present the characteristics of the first- and second-order ac specific heats of the glass former and show that the glass transition temperature, the Vogel–Fulcher temperature and the crossover temperature can be determined by the ac specific heats. In section 6, our conclusion is given.

2. The first- and second-order specific heats

The specific heat at the constant volume C_V is conventionally defined by a derivative of the energy with respect to the temperature,

$$C_V(T) = \left(\frac{\partial E_{\rm eq}}{\partial T}\right)_V, \tag{2}$$

where $E_{\rm eq}$ is the energy in the equilibrium state, T is the temperature and V is the volume. In this discussion of the specific heat, it is not considered how long the system takes to equilibrate itself when the temperature is changed. When the system contains degrees of freedom of slow dynamics, one must consider the effect of the delay in response. We consider the energy response of a system with slow relaxations which is subjected to a heat bath whose temperature is oscillated as $T + \Delta T(t)$, where T is the average temperature and $\Delta T(t)$ is the oscillating part. We assume that the energy response $\Delta E(t)$ can be expanded as follows:

$$\begin{aligned}\Delta E(t) = &\int_{-\infty}^{t} {\rm d}t_1\, C_1(t-t_1)\Delta T(t_1)\\ &+ \int_{-\infty}^{t}{\rm d}t_1\int_{-\infty}^{t}{\rm d}t_2\, C_2(t-t_1, t-t_2)\\ &\times \Delta T(t_1)\Delta T(t_2) + {\rm O}(\Delta T^3),\end{aligned} \tag{3}$$

where C_1 and C_2 represent the retardation effect of the system.

The Fourier transform $\Delta E(\omega)$ of equation (3) is given by

$$\begin{aligned}\Delta E(\omega) = &\tilde{C}_1({\rm i}\omega)\Delta T(\omega) + \int_{-\infty}^{\infty}{\rm d}\omega_1\, \tilde{C}_2({\rm i}\omega_1, {\rm i}\omega - {\rm i}\omega_1)\\ &\times \Delta T(\omega_1)\Delta T(\omega-\omega_1) + {\rm O}(\Delta T^3)\end{aligned} \tag{4}$$

where the Laplace components $\tilde{C}_1(p)$ and $\tilde{C}_2(p_1, p_2)$ are defined by

$$\tilde{C}_1(p) = \int_0^{\infty}{\rm d}t\, C_1(t){\rm e}^{-pt}, \tag{5}$$

$$\tilde{C}_2(p_1, p_2) = \int_0^{\infty}{\rm d}t_1\int_0^{\infty}{\rm d}t_2\, C_2(t_1, t_2){\rm e}^{-p_1t_1}{\rm e}^{-p_2t_2}, \tag{6}$$

and $\Delta T(\omega)$ is the Fourier transform of $\Delta T(t)$.

We now discuss the energy response $\Delta E(t)$ when $\Delta T(t)$ is a sinusoidal function $\Delta T(t) = T_{\rm a}\sin(\omega t)$, where $T_{\rm a}$ is the amplitude of the oscillating temperature. It is straightforward to show that

$$\begin{aligned}\Delta E(t) = &T_{\rm a}\{\tilde{C}_1'({\rm i}\omega)\sin(\omega t) + \tilde{C}_1''({\rm i}\omega)\cos(\omega t)\}\\ &- \frac{T_{\rm a}^2}{2}\{\tilde{C}_2'({\rm i}\omega, {\rm i}\omega)\cos(2\omega t) - \tilde{C}_2''({\rm i}\omega, {\rm i}\omega)\sin(2\omega t)\\ &- \tilde{C}_2'({\rm i}\omega, -{\rm i}\omega)\} + {\rm O}(T_{\rm a}^3).\end{aligned} \tag{7}$$

Here $C_1(t)$ and $C_2(t_1, t_2)$ are assumed to be real and the notations $'$ and $''$ represent the real and imaginary parts, respectively. The coefficients of the first-order temperature term, $\tilde{C}_1'({\rm i}\omega)$ and $\tilde{C}_1''({\rm i}\omega)$, are known as the real and imaginary parts of the (first-order) ac specific heat, which was introduced by Birge and Nagel [16] and by Christensen [17].

The second-order temperature term consists of the oscillating and non-oscillating terms. We define the second-order ac specific heat $\tilde{C}_2'({\rm i}\omega, {\rm i}\omega)$ and $\tilde{C}_2''({\rm i}\omega, {\rm i}\omega)$ by the coefficients of the oscillating term.

The Laplace–Fourier transforms $\tilde{C}_1(p)$ and $\tilde{C}_2(p_1, p_2)$ are related to the temperature derivative of the energy. When the change of the temperature is slower than that of the timescale of the retardation effects $C_1(t)$ and $C_2(t_1, t_2)$, it is straightforward to obtain the following expressions:

$$\lim_{p\to 0}\tilde{C}_1(p) = \int_0^{\infty}{\rm d}t\, C_1(t) = \frac{\partial E_{\rm eq}}{\partial T} \tag{8}$$

$$\begin{aligned}&\lim_{p_1\to 0}\lim_{p_2\to 0}\tilde{C}_2(p_1, p_2)\\ &= \int_0^{\infty}{\rm d}t_1\int_0^{\infty}{\rm d}t_2\, C_2(t_1, t_2) = \frac{1}{2}\frac{\partial^2 E_{\rm eq}}{\partial T^2}.\end{aligned} \tag{9}$$

When the frequency is smaller than the inverse of the structural relaxation time, the energy responses without delay and $\Delta E(t)$ can be expressed as

$$\Delta E(t) = \frac{\partial E_{\rm eq}}{\partial T}\Delta T(t) + \frac{1}{2}\frac{\partial^2 E_{\rm eq}}{\partial T^2}\Delta T^2(t) + {\rm O}(\Delta T^3). \tag{10}$$

In this limit, $\tilde{C}_1'(\mathrm{i}\omega)$ becomes equal to the specific heat in the equilibrium state, $C_V = \partial E_{\mathrm{eq}}/\partial T$ and $\tilde{C}_1''(\mathrm{i}\omega)$ vanishes. It can also be confirmed that in this limit $\tilde{C}_2(\mathrm{i}\omega, \mathrm{i}\omega)$ and $\tilde{C}_2(\mathrm{i}\omega, -\mathrm{i}\omega)$ correspond to the temperature derivative of the specific heat. These behaviors are consistent with equations (8) and (9).

3. Dynamics on the free energy landscape

The free energy surface in the configurational space is defined by the partial partition function, which is given by the partial summation of the phase space spanned by the fast microscopic motion [5, 6], and the slow dynamics is represented by the stochastic motion on the free energy surface. Around the glass transition point, the stochastic motions can be classified into two types: the fluctuation in one basin due to the structural fluctuation around a certain structure and the transition between basins which corresponds to the structural relaxation.

Here, we concentrate on the transition between basins and ignore the fluctuation within a single basin. We denote the probability that the system is in basin i at time t at temperature T by $P_i(T, t)$ and a physical quantity A of basin i by $A_i(T)$. Then the physical quantity we measure at time t is defined as an average over the basins,

$$A(T, t) = \sum_i A_i(T) P_i(T, t) = \vec{A}(T) \cdot \vec{P}(T, t), \tag{11}$$

where $\vec{A}(T)$ and $\vec{P}(T, t)$ are the vectors consisting of components $A_i(T)$ and $P_i(T, t)$, respectively.

The probability vector $\vec{P}(T, t)$ is assumed to obey the master equation,

$$\frac{\mathrm{d}}{\mathrm{d}t}\vec{P}(T, t) = W(T)\vec{P}(T, t), \tag{12}$$

where $W(T)$ is the transition rate matrix, i.e. W_{ij} is the transition rate from basin j to i and $W_{ii} = -\sum_{j\neq i} W_{ji}$ is the transition rate jumping out from basin i. The transition rate is assumed to be related to the free energy barrier as follows:

$$W_{ij} = C \exp[-\beta(F_A(T) - F_j(T))], \tag{13}$$

where C is the attempt frequency of the jump motion, $\beta = 1/k_{\mathrm{B}}T$ is the inverse of the temperature T multiplied by the Boltzmann constant k_{B}, $F_i(T)$ is the free energy of basin i, $F_A(T) = \max\{F_i(T), F_j(T)\} + \Delta_{i,j}(T)$ and $\Delta_{i,j}(T)$ is the energy barrier between basins i and j. In the high temperature region, the transition rate is large and the system moves among basins freely. On the other hand, the transition rate becomes small and the structural transition is hindered at low temperatures.

The transition rate matrix W in the master equation (12) must satisfy the condition that the long time limit of $P_i(T, t)$ becomes the Boltzmann distribution

$$\lim_{t\to\infty} P_i(T, t) = P_i^{\mathrm{eq}}(T) = \frac{\exp[-\beta F_i(T)]}{\sum_j \exp[-\beta F_j(T)]}. \tag{14}$$

Therefore, the transition rate matrix W obeys the following detailed balance:

$$W\vec{P}^{\mathrm{eq}} = 0. \tag{15}$$

When the temperature T does not depend on time, equation (12) can be readily solved,

$$\begin{aligned}\vec{P}(T, t) &= \exp[W(T)t]\vec{P}(T, t = 0)\\ &= V\begin{pmatrix}\exp(\lambda_1 t) & & & \\ & \ddots & & \\ & & \exp(\lambda_{N-1}t) & \\ & & & \exp(\lambda_N t)\end{pmatrix}\\ &\quad\times V^{-1}\vec{P}(T, t = 0),\end{aligned} \tag{16}$$

where N is the number of basins, λ_i is the ith eigenvalue of W and V is a matrix whose columns are eigenvectors of W. It is important to note that there is an eigenvalue $\lambda_i = 0$ which corresponds to the detailed balance of equation (15).

4. The energy response to the oscillating temperature

4.1. The first- and second-order energy response

The time dependent temperature $\hat{T}(t)$ is assumed to be $\hat{T}(t) = T + \Delta T(t)$, where T is the average temperature and $\Delta T(t)$ is the oscillating part of the temperature. The probability vector $\vec{P}(T, t)$ is expanded as

$$\vec{P}(\hat{T}(t), t) = \vec{P}_0(t) + \Delta\vec{P}_1(t) + \Delta\vec{P}_2(t) + \mathrm{O}(\Delta T^3), \tag{17}$$

where $\Delta\vec{P}_n$ is the term of order ΔT^n. Note that the explicit temperature dependence of the quantities on the right-hand side of equation (17) is omitted. It is clear that $\vec{P}_0(t) = \vec{P}^{\mathrm{eq}}(T)$. Then the first- and second-order energy responses, $\Delta E_1(t)$ and $\Delta E_2(t)$, at time t are represented as

$$\Delta E_1(t) = \vec{E}\cdot\Delta\vec{P}_1(t) + \frac{\partial\vec{E}}{\partial T}\cdot\vec{P}_{\mathrm{eq}}(T)\Delta T(t) \tag{18}$$

$$\begin{aligned}\Delta E_2(t) &= \vec{E}\cdot\Delta\vec{P}_2(t) + \frac{\partial\vec{E}}{\partial T}\Delta\vec{P}_1(t)\Delta T(t)\\ &\quad + \frac{1}{2}\frac{\partial^2\vec{E}}{\partial T^2}\vec{P}_{\mathrm{eq}}(T)\Delta T^2(t)\end{aligned} \tag{19}$$

where $\vec{E}$ is the vector consisting of components E_i. The first- and second-order probability responses, $\Delta P_1(t)$ and $\Delta P_2(t)$, obey the following equations derived from equation (12):

$$\frac{\mathrm{d}}{\mathrm{d}t}\Delta\vec{P}_1(t) = W(T)\Delta\vec{P}_1(t) + \frac{\partial W(T)}{\partial T}\vec{P}_{\mathrm{eq}}(T)\Delta T(t) \tag{20}$$

$$\begin{aligned}\frac{\mathrm{d}}{\mathrm{d}t}\Delta\vec{P}_2(t) &= W(T)\Delta\vec{P}_2(t) + \frac{\partial W(T)}{\partial T}\Delta\vec{P}_1(t)\Delta T(t)\\ &\quad + \frac{1}{2}\frac{\partial^2 W(T)}{\partial T^2}\vec{P}_{\mathrm{eq}}(T)\Delta T(t)^2.\end{aligned} \tag{21}$$

It is straightforward to solve equations (20) and (21) as

$$\Delta\vec{P}_1(t) = \int_{-\infty}^{t}\mathrm{d}s\,\mathrm{e}^{W(t-s)}\frac{\partial W}{\partial T}\vec{P}_{\mathrm{eq}}(T)\Delta T(s), \tag{22}$$

$$\begin{aligned}\Delta\vec{P}_2(t) &= \int_{-\infty}^{t}\mathrm{d}s_1\int_{-\infty}^{s_1}\mathrm{d}s_2\,\mathrm{e}^{W(t-s_1)}\frac{\partial W}{\partial T}\mathrm{e}^{W(s_1-s_2)}\frac{\partial W}{\partial T}\vec{P}_{\mathrm{eq}}(T)\\ &\quad\times\Delta T(s_1)\Delta T(s_2) + \frac{1}{2}\int_{-\infty}^{t}\mathrm{d}s\,\mathrm{e}^{W(t-s)}\frac{\partial^2 W}{\partial T^2}\Delta T^2(s).\end{aligned} \tag{23}$$

4.2. The first-order energy response and the ac specific heat

The (first-order) ac specific heat is defined as the linear coefficient of the energy response to the temperature change [12]. Comparing equations (3), (18) and (22), the retardation effect of the first-order energy response $C_1(t)$ is represented in the free energy landscape picture as follows:

$$C_1(t) = 2C_0(T)\delta(t) + \vec{E}\cdot\exp(Wt)\frac{\partial W}{\partial T}\vec{P}_{\rm eq}, \qquad (24)$$

where $C_0(T) = \vec{P}_{\rm eq}\cdot\partial\vec{E}/\partial T$ is the quenched specific heat contributed only from the fast degree of freedom at one basin [8–11, 14]. The second term represents the response from the transition between basins.

From equation (5), the first-order ac specific heat $\tilde{C}_1(\mathrm{i}\omega)$ is given by the Laplace–Fourier transform of $C_1(t)$.

$$\tilde{C}_1(\mathrm{i}\omega) = \frac{\partial\vec{E}}{\partial T}\cdot\vec{P}_{\rm eq} + \mathrm{i}\omega\vec{E}\cdot(\mathrm{i}\omega - W)^{-1}\frac{\partial\vec{P}_{\rm eq}}{\partial T}. \qquad (25)$$

The real part $\tilde{C}_1'(\mathrm{i}\omega)$ and the imaginary part $\tilde{C}_1''(\mathrm{i}\omega)$ are written as

$$\begin{aligned}\tilde{C}_1'(\mathrm{i}\omega) &= C_0(T) + \vec{E}\cdot V \\ &\times \begin{pmatrix}\lambda_1^2/(\omega^2+\lambda_1^2) & & \\ & \ddots & \\ & & \lambda_N^2/(\omega^2+\lambda_N^2)\end{pmatrix} \\ &\times V^{-1}\frac{\partial\vec{P}_{\rm eq}}{\partial T}, \qquad (26)\\ \tilde{C}_1''(\mathrm{i}\omega) &= \vec{E}\cdot V \\ &\times \begin{pmatrix}\lambda_1\omega/(\omega^2+\lambda_1^2) & & \\ & \ddots & \\ & & \lambda_N\omega/(\omega^2+\lambda_N^2)\end{pmatrix} \\ &\times V^{-1}\frac{\partial\vec{P}_{\rm eq}}{\partial T}. \qquad (27)\end{aligned}$$

The frequency dependence of the ac specific heat is shown in figure 1 schematically. In the low frequency region, $\tilde{C}_1'(\mathrm{i}\omega)$ approaches the specific heat in the equilibrium state as $C_{\rm eq}(T) = \partial\vec{E}/\partial T\cdot\vec{P}^{\rm eq} + \vec{E}\cdot\partial\vec{P}^{\rm eq}/\partial T$ and $\tilde{C}_1''(\mathrm{i}\omega)$ vanishes. This indicates the fact that the energy responds without time delay when the temperature is oscillated slowly. Since the eigenvalue λ_i is distributed, $\tilde{C}_1''(\mathrm{i}\omega)$ has a broader peak than that of the Debye relaxation type and $\tilde{C}_1'(\mathrm{i}\omega)$ is represented as the sum of Lorentzian functions. This behavior is consistent with the measurement of the ac specific heat in glass forming materials [16]. In the high frequency region, $\tilde{C}_1'(\mathrm{i}\omega)$ approaches $C_0(T)$ and $\tilde{C}_1''(\mathrm{i}\omega)$ vanishes. This exhibits that the energy response within the first-order temperature perturbation is determined by the energy change in a basin alone when the temperature fluctuates rapidly.

The first-order ac specific heat can be used as the method to obtain the statistics of eigenvalues λ_i. From equations (26) and (27), the scaled first-order ac specific heat is related to the distribution of the eigenvalues λ_i of the transition rate matrix as follows:

$$\frac{\tilde{C}_1'(\mathrm{i}\omega) - C_0}{C_{\rm eq} - C_0} = \sum_i g_i\frac{\lambda_i^2}{\lambda_i^2+\omega^2}, \qquad (28)$$

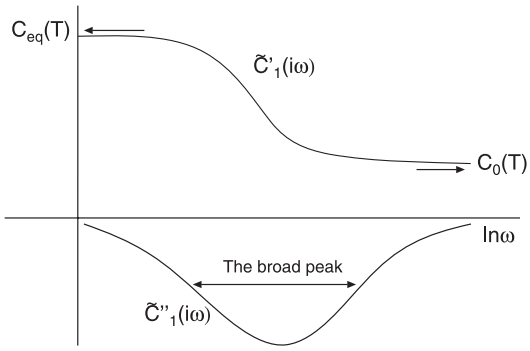

Figure 1. The schematic picture of the (first-order) ac specific heat in the free energy landscape picture.

$$\frac{\tilde{C}_1''(\mathrm{i}\omega)}{C_{\rm eq} - C_0} = \sum_i g_i\frac{\lambda_i\omega}{\omega^2+\lambda_i^2}. \qquad (29)$$

Here, g_i is a factor related to the vectors $\vec{E}$, $\vec{P}_{\rm eq}$ and V given by

$$g_i = \frac{\sum_{j,k}E_iV_{ji}V_{ik}^{-1}\frac{\partial P_{\rm eq}^k}{\partial T}}{C_{\rm eq} - C_0}. \qquad (30)$$

In the small frequency region, the imaginary part behaves as $\lim_{\omega\to0}\tilde{C}_1''(\mathrm{i}\omega)/(C_{\rm eq} - C_0) = \sum_i g_i\lambda_i^{-1}\omega$. In the high frequency region, the real part behaves as $\lim_{\omega\to\infty}(\tilde{C}_1'(\mathrm{i}\omega) - C_0)/(C_{\rm eq} - C_0) = \sum_i g_i\lambda_i^2/\omega^2$ and the imaginary part behaves as $\lim_{\omega\to\infty}\tilde{C}_1''(\mathrm{i}\omega)/(C_{\rm eq} - C_0) = \sum_i g_i\lambda_i\omega^{-1}$. We can estimate $\sum_i g_i\lambda_i$, $\sum_i g_i\lambda_i^2$ and $\sum_i g_i\lambda_i^{-1}$ from the frequency dependence of the scaled first-order ac specific heat. These properties correspond to $\langle\lambda\rangle$, $\langle\lambda^2\rangle$ and $\langle\lambda^{-1}\rangle$ respectively, as will be shown in section 5.

4.3. The second-order ac specific heat

The retardation effect of the second-order energy response $C_2(t_1, t_2)$ is represented from equations (3), (19) and (23) as

$$\begin{aligned}C_2(t_1,t_2) &= 2\frac{\partial C_0}{\partial T}\delta(t_1)\delta(t_2) + \vec{E}\cdot\exp(Wt_1)\frac{\partial W}{\partial T}\exp(Wt_2) \\ &\times\frac{\partial W}{\partial T}\vec{P}^{\rm eq}\theta(t_2-t_1) + \frac{1}{2}\vec{E}\cdot\exp(Wt_1)\frac{\partial^2 W}{\partial T^2}\vec{P}^{\rm eq}\delta(t_1-t_2) \\ &+ 2\frac{\partial\vec{E}}{\partial T}\exp(Wt_1)\frac{\partial W}{\partial T}\vec{P}^{\rm eq}\delta(t_2). \qquad (31)\end{aligned}$$

The first term expresses the response due to the instant change of the specific heat of each basin and the remaining terms correspond to the effect of the transition motion between basins. Here, $\delta(x)$ is the Dirac delta function and $\theta(x)$ is the Heaviside step function.

From definition (6), the Laplace transform $\tilde{C}_2(p_1, p_2)$ is represented as

$$\begin{aligned}\tilde{C}_2(p_1,p_2) &= \frac{1}{2}\frac{\partial C_{\rm eq}}{\partial T} - p_2\vec{E}\cdot((p_1+p_2)\hat{1} - W)^{-1} \\ &\times\frac{\partial W}{\partial T}(p_2\hat{1} - W)^{-1}\frac{\partial\vec{P}^{\rm eq}}{\partial T} - \frac{p_1+p_2}{2}\end{aligned}$$

$$\times \vec{E} \cdot ((p_1 + p_2)\hat{1} - W)^{-1} \frac{\partial^2 \vec{P}^{\rm eq}}{\partial T^2}$$

$$- p_1 \frac{\partial \vec{E}}{\partial T}(p_1\hat{1} - W)^{-1} \frac{\partial \vec{P}^{\rm eq}}{\partial T}. \quad (32)$$

The second-order ac specific heats, which are introduced in equation (3) by the coefficients of the oscillating term in the second-order energy response, $\tilde{C}_2(\mathrm{i}\omega, \mathrm{i}\omega) = \tilde{C}_2'(\mathrm{i}\omega, \mathrm{i}\omega) + \mathrm{i}\tilde{C}_2''(\mathrm{i}\omega, \mathrm{i}\omega)$, are expressed as

$$\tilde{C}_2'(\mathrm{i}\omega, \mathrm{i}\omega) = \frac{1}{2}\frac{\partial C_{\rm eq}}{\partial T} - 2\omega^2 \vec{E} \cdot (W^2 + 4\omega^2)^{-1} \frac{\partial^2 \vec{P}^{\rm eq}}{\partial T^2}$$

$$+ \omega^2 \vec{E} \cdot (W^2 + 4\omega^2)^{-1} \left\{ 2\frac{\partial W}{\partial T} W + W \frac{\partial W}{\partial T} \right\}$$

$$\times (W^2 + \omega^2)^{-1} \frac{\partial \vec{P}^{\rm eq}}{\partial T} - \omega^2 \frac{\partial \vec{E}}{\partial T}(W^2 + \omega^2)^{-1} \frac{\partial \vec{P}^{\rm eq}}{\partial T}, \quad (33)$$

$$\tilde{C}_2''(\mathrm{i}\omega, \mathrm{i}\omega) = \omega \vec{E} \cdot W(W^2 + 4\omega^2)^{-1} \frac{\partial^2 \vec{P}^{\rm eq}}{\partial T^2}$$

$$+ \omega \vec{E} \cdot (W^2 + 4\omega^2)^{-1} \left\{ 2\omega^2 \frac{\partial W}{\partial T} - W \frac{\partial W}{\partial T} W \right\}$$

$$\times (W^2 + \omega^2)^{-1} \frac{\partial \vec{P}^{\rm eq}}{\partial T} + \omega \frac{\partial \vec{E}}{\partial T}(W^2 + \omega^2)^{-1} \frac{\partial \vec{P}^{\rm eq}}{\partial T}. \quad (34)$$

In the low frequency limit, $\tilde{C}_2'(\mathrm{i}\omega, \mathrm{i}\omega)$ becomes $(\partial C_{\rm eq}/\partial T)/2$ and $\tilde{C}_2''(\mathrm{i}\omega, \mathrm{i}\omega)$ vanishes. In the high frequency limit, $\tilde{C}_2'(\mathrm{i}\omega, \mathrm{i}\omega)$ is equal to $(\partial C_0/\partial T)/2$ and $\tilde{C}_2''(\mathrm{i}\omega, \mathrm{i}\omega)$ vanishes. These behaviors are qualitatively similar to those of the first-order ac specific heat. It indicates that the structural change of the system can catch up with the temperature change in the small frequency region and cannot in the high frequency region.

Terms including the differential of the transition rate with respect to the temperature, $\partial W/\partial T$, are expected to show the characteristic behavior in the low temperature region, where the transition matrix W depends strongly on the temperature change. This characteristic does not appear in the first-order ac specific heat. In the high temperature region, the temperature dependence of the transition rate matrix W is weak. Therefore, the terms including $\partial W/\partial T$ are negligible, and the second-order ac specific heat becomes the superposition of the susceptibility of the Debye relaxation. We explain this behavior for a trap model in the next section.

The second-order energy response can be measured in the materials where the derivatives of the quenched and equilibrium specific heats are very different, since the order of the second-order energy response is the difference between derivatives of these specific heats, $\partial(C_{\rm eq} - C_0)/\partial T$.

The ac specific heat is often estimated from the measurement of the temperature response to the oscillating heat flow. The second-order ac specific heat can be also measured from the temperature response. We explain the relation in the appendix.

5. Application to a model free energy landscape of glass forming systems

5.1. Model

To clarify the characteristics of the first- and second-order ac specific heat of glass forming materials, we apply the present analysis of the ac specific heat to a model landscape incorporated with the distribution of the transition rate exploited in the trapping diffusion model [7, 19].

We prepare a landscape consisting of 20 basins which are mutually connected. The microscopic dynamics of the system in each basin is assumed to be the Debye oscillator. The free energy, F_i, of basin i is given by

$$F_i = \epsilon_i + \exp\left\{ 9\left(\frac{T}{\Theta_D}\right)^3 \int_0^{\Theta_D/T} \ln\left(\frac{1}{2}\sin^{-1}\frac{x}{2}\right) x^2 \,\mathrm{d}x \right\}, \quad (35)$$

where the energy ϵ_i of the bottom of basin i is uniformly distributed with the variance ϵ and Θ_D is the Debye temperature. Note that the form of the distribution does not play any important role in the following discussion.

The energy, E_i, of basin i is calculated from the temperature derivative of the free energy F_i. The transition rate w is assumed to obey the power law distribution $P(w)$ as in the trapping diffusion model [7, 19],

$$P(w) = \begin{cases} \dfrac{\rho + 1}{w_0}\left(\dfrac{w}{w_0}\right)^{\rho} & (0 \leqslant w \leqslant w_0) \\ 0 & \text{otherwise,} \end{cases} \quad (36)$$

where ρ is related to the configurational entropy $S_{\rm c}(T)$ as

$$\rho = \frac{T S_{\rm c}(T) - T_{\rm g} S_c(T_{\rm g})}{T_{\rm g} S_c(T_{\rm g})}. \quad (37)$$

The transition rate from basin j to i, W_{ij}, is now a random variable given by

$$W_{ij} = w_0 x^{\frac{1}{\rho+1}} \exp[-\beta(F_A(T) - F_j(T))]$$
$$= w_0 x^{\frac{T_{\rm g} S_c(T_{\rm g})}{T S_{\rm c}(T)}} \exp[-\beta(F_A(T) - F_j(T))]. \quad (38)$$

Here, x is the uniform random number in [0, 1].

When the temperature is decreased towards T_0 and $S_{\rm c}(T)$ vanishes, two important aspects are pointed out from the temperature dependence of W_{ij}: (1) W_{ij} approaches zero and (2) the derivative of W_{ij} with respect to the temperature $\partial W_{ij}/\partial T$ has a diverging term,

$$-\frac{\log x T_{\rm g} S_c(T_{\rm g})}{(T S_{\rm c}(T))^2} \frac{\partial (T S_{\rm c}(T))}{\partial T} W_{ij}. \quad (39)$$

The characteristic behaviors of the ac specific heats are related to these aspects. (1) The first-order ac specific heat has a peak which shifts to the low frequency region and (2) the second-order ac specific heat has a diverging peak related to the diverging term of the temperature derivative of W_{ij}. (See equations (33) and (34).)

For numerical calculations in this study, the exponent ρ of the jump rate distribution is simplified as

$$\rho = \frac{T - T_{\rm g}}{T_{\rm g} - T_0}, \quad (40)$$

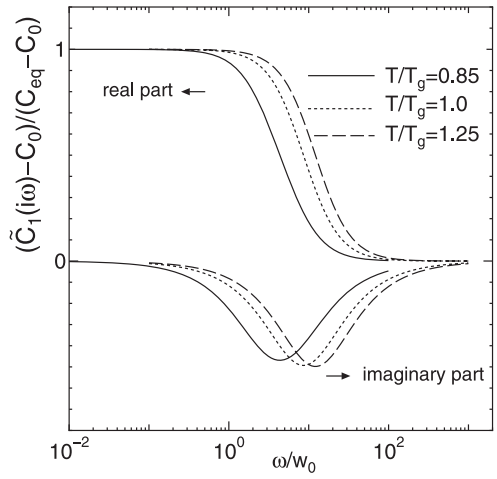

Figure 2. The scaled ac specific heat in the trap model at the temperature $T/T_{\rm g} = 0.85$ (solid line), 1.0 (dotted line), 1.25 (dashed line).

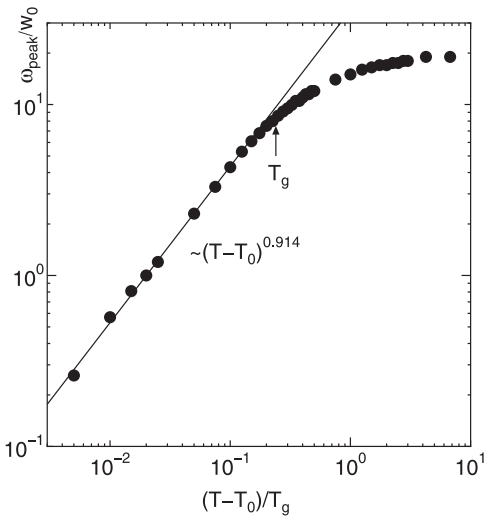

Figure 3. The temperature dependence of the frequency at the peak of the imaginary part of the first-order ac specific heat: the peak frequency (black circle) becomes small as the temperature reduces towards the Vogel–Fulcher temperature T_0. The line is fitted with the data in the low temperature region.

i.e. the configurational entropy $S_{\rm c}(T)$ is assumed as $TS_{\rm c}(T) \propto T - T_0$ with the Vogel–Fulcher temperature $T_0 \sim T_k$ and the parameters are chosen as $T_0/T_{\rm g} = 0.75$ and $\Theta_D/T_{\rm g} = 12.5$, respectively. In addition, the crossover temperature T_x is $T_x/T_{\rm g} = 1.25$, since the crossover temperature is identified with the exponent $\rho = 1.0$ [19].

5.2. The first-order ac specific heat

The real and imaginary parts of the scaled first-order ac specific heat $(\tilde{C}_1(\mathrm{i}\omega) - C_0)/(C_{\rm eq} - C_0)$ are shown in figure 2. As the temperature is reduced, a peak of the imaginary part shifts to the low frequency region and the width of the peak increases.

Figure 3 shows the temperature dependence of the frequency $\omega_{\rm peak}$ at the peak of the imaginary part. In the low temperature region below $T_{\rm g}$, $\omega_{\rm peak}$ obeys the power law function as $\omega_{\rm peak} \sim (T - T_0)^{0.914}$. In the high temperature region above $T_{\rm g}$, the temperature dependence changes and $\omega_{\rm peak}$ approaches towards $20w_0$. It is straightforward to show that, when N basins are mutually connected, the $\omega_{\rm peak}$ becomes Nw_0 in the high temperature region. In fact from equation (38), all transition rates are w_0 when the temperature is much higher than the glass transition temperature $T_{\rm g}$. The relaxation time due to eigenvalues of the transition matrix W is not distributed and the first-order ac specific heat becomes the same as the susceptibility of the Debye relaxation. The master equation (12) can be solved without difficulties in this limit as $P_i(T,t) = \mathrm{e}^{-Nw_0t}(P_i(t=0) - 1/N) + 1/N$. Thus the peak frequency $\omega_{\rm peak}$ becomes Nw_0 in the high temperature region.

We define the stretching factor σ by the ratio $\sigma \equiv \omega_+/\omega_-(\omega_+ > \omega_-)$. Here, $\omega_\pm$ is the frequency satisfying the relation $\tilde{C}_1''(\mathrm{i}\omega_\pm) = \tilde{C}_1''(\mathrm{i}\omega_{\rm peak})/2$. Figure 4 shows the stretching factor σ as a function of temperature. In the high temperature region above $T_{\rm g}$, σ is the same as that of the Debye susceptibility. As the temperature is reduced towards T_0, σ of the peak increases and diverges at T_0. This means that the relaxation time is distributed and the broad peak appears in

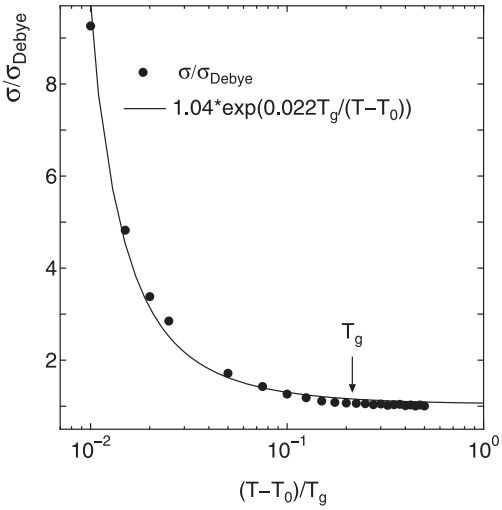

Figure 4. The temperature dependence of the stretching factor σ of the imaginary part. The line represents the fitted line by the Vogel–Fulcher law. Here, $\sigma_{\rm Debye} = (2+\sqrt{3})/(2-\sqrt{3})$ is the stretching factor for the Debye relaxation type. As the temperature is reduced towards the Vogel–Fulcher temperature T_0, σ increases.

$\tilde{C}_1''(\mathrm{i}\omega)$ below $T_{\rm g}$. It is interesting to note that σ can be fitted well by the Vogel–Fulcher law as $\sigma \sim \exp(A/(T-T_0))$ shown in figure 4.

The statistics of eigenvalues of the transition rate matrix W can be obtained from the frequency dependence of $\tilde{C}_1(\mathrm{i}\omega)$ (see section 4.2). We show a result of comparison of $\lim_{\omega\to\infty}\omega\tilde{C}_1''(\mathrm{i}\omega)/(C_{\rm eq} - C_0)$, $\lim_{\omega\to\infty}\omega^2(\tilde{C}_1'(\mathrm{i}\omega) - C_0)/(C_{\rm eq} - C_0)$, and $\lim_{\omega\to 0}\omega^{-1}\tilde{C}_1''(\mathrm{i}\omega)/(C_{\rm eq} - C_0)$ with statistics of eigenvalues $\langle\lambda\rangle$, $\langle\lambda^2\rangle$ and $\langle\lambda^{-1}\rangle$ in figure 5. Here, $\langle f(\lambda)\rangle$ represents the statistics of eigenvalues as $\langle f(\lambda)\rangle = \sum_{i=1,\lambda_i\neq 0}^{20} f(\lambda_i)/20$, which is calculated numerically from the transition matrix W. The result indicates that the contribution

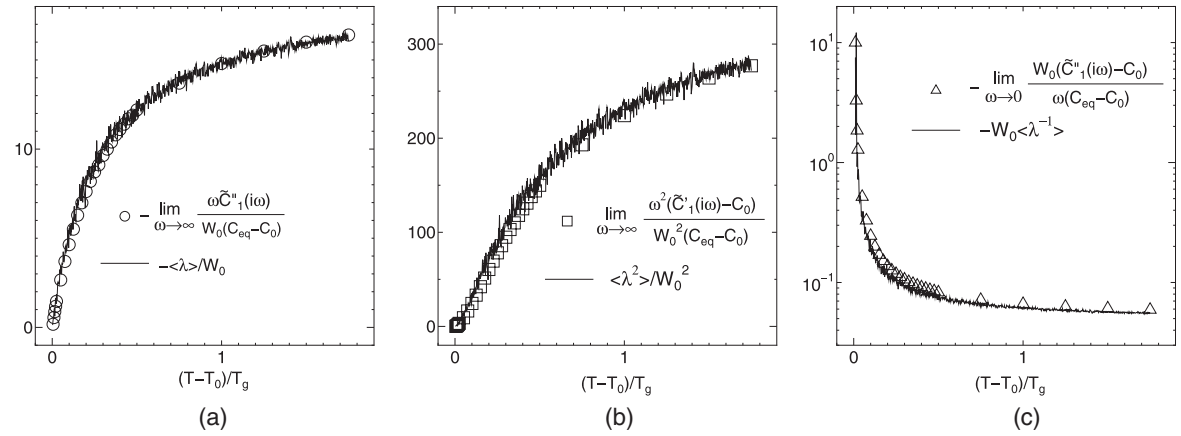

Figure 5. The temperature dependence of (a) $-\lim_{\omega\to\infty}\omega\tilde{C}_1''(\mathrm{i}\omega)/(C_{\mathrm{eq}}-C_0)/W_0$, (b) $\lim_{\omega\to\infty}\omega^2(\tilde{C}_1'(\mathrm{i}\omega)-C_0)/(C_{\mathrm{eq}}-C_0)/W_0^2$ and (c) $-W_0\lim_{\omega\to 0}\omega^{-1}(\tilde{C}_1''(\mathrm{i}\omega)-C_0)/(C_{\mathrm{eq}}-C_0)$ determined from the frequency dependence of the first-order ac specific heat. The solid lines represent (a) $-\langle\lambda\rangle/W_0$, (b) $\langle\lambda^2\rangle/W_0^2$ and (c) $-W_0\langle\lambda^{-1}\rangle$, which are calculated numerically from eigenvalues of the transition matrix W, respectively.

of g_i is negligible and the coefficients obtained from the frequency dependence of the first-order ac specific heat can be used to estimate the statistics of eigenvalues of the transition rate matrix.

Figure 6 shows the temperature dependence of $\lim_{\omega\to\infty}\omega\tilde{C}_1''(\mathrm{i}\omega)/(C_{\mathrm{eq}}-C_0)/W_0$, $\lim_{\omega\to\infty}\{\omega^2(\tilde{C}_1'(\mathrm{i}\omega)-C_0)/(C_{\mathrm{eq}}-C_0)/W_0^2\}^{1/2}$ and $\lim_{\omega\to 0}\omega(C_{\mathrm{eq}}-C_0)/(\tilde{C}_1'(\mathrm{i}\omega)-C_0)/W_0$; the deviation between these statistics becomes significant below T_{g}. This reflects that the distribution of the eigenvalues becomes broader below T_{g}.

5.3. The second-order ac specific heat

The real and imaginary parts of the scaled second-order ac specific heat $(\tilde{C}_2(\mathrm{i}\omega,\mathrm{i}\omega)-\tilde{C}_2(\mathrm{i}\infty,\mathrm{i}\infty))/(\tilde{C}_2(0,0)-\tilde{C}_2(\mathrm{i}\infty,\mathrm{i}\infty))$ are shown in figures 7 and 8, respectively. The real part shows a decreasing local minimum when the temperature is reduced below the crossover temperature $T_x/T_{\mathrm{g}}=1.25$. It is important to note that similar behavior is shown for the imaginary part in figure 8, where the imaginary part has a decreasing minimum and an increasing maximum below the crossover temperature.

The deviation from the Debye relaxation appears clearly in the Cole–Cole plot of the second-order ac specific heat shown in figure 9. In the high temperature region, the plots show a semicircle, since the second-order ac specific heat is equal to the susceptibility of the Debye relaxation. As the temperature is reduced, the plots deviate from a semicircle, that shows that the terms including $\partial W/\partial T$ in equations (33) and (34) give significant contributions.

The temperature dependence of the extrema of the second-order ac specific heat is shown in figure 10. Below T_{g}, the extrema obey the power law as $(T-T_0)^{-\nu}$ as the temperature is decreased towards T_0, at which the configurational entropy vanishes. The exponents ν are $\nu=0.97, 1.05, 1.01$ for the local maximum of the real part, the local minimum and the local maximum of the imaginary part, respectively. Above T_{g}, the temperature dependence of the minimum of the imaginary part deviates from the power law and approaches a constant value.

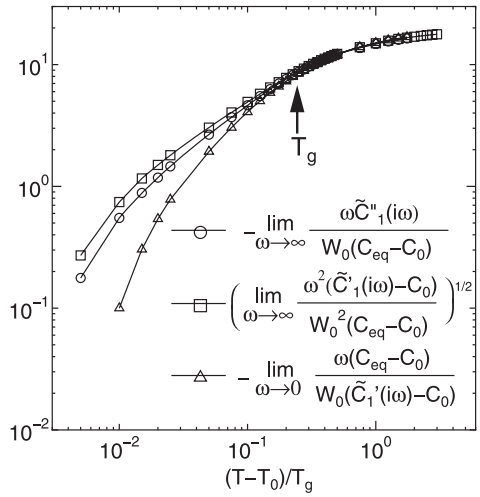

Figure 6. The temperature dependence of $-\lim_{\omega\to\infty}\omega\tilde{C}_1''(\mathrm{i}\omega)/(C_{\mathrm{eq}}-C_0)/W_0$, $\lim_{\omega\to\infty}\{\omega^2(\tilde{C}_1'(\mathrm{i}\omega)-C_0)/(C_{\mathrm{eq}}-C_0)/W_0^2\}^{1/2}$ and $-\lim_{\omega\to 0}\omega(C_{\mathrm{eq}}-C_0)/(\tilde{C}_1'(\mathrm{i}\omega)-C_0)/W_0$. The deviation of these properties becomes significant below T_{g}.

6. Conclusion

We have presented the theoretical formalism of calculating the energy response to the oscillating temperature in the free energy landscape picture. The characteristic behaviors of the energy responses are summarized as follows.

The large and small frequency limits of the first-order ac specific heat are identical to the equilibrium and quenched specific heat in the free energy landscape picture, respectively. Similar behavior appears in the second-order ac specific heat. The large and small frequency limits of the second-order ac specific heat are identical to the temperature derivative of the annealed and quenched specific heat, respectively. The distribution of the eigenvalues of the transition rate matrix among basins is shown to give rise to a broad peak of the imaginary part of the first-order ac specific heat. This is consistent with the experiment for the glass forming materials.

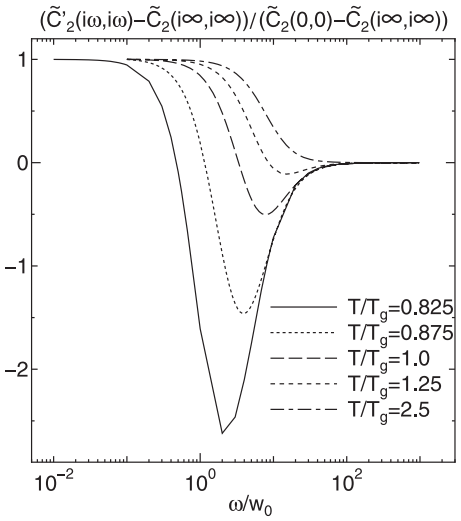

Figure 7. The real part of the scaled second-order ac specific heat at temperatures $T/T_g = 0.825$, 0.875, 1.0, 1.25 and 2.5: As the temperature is decreased below the temperature $T_x/T_g = 1.25$, a local minimum decreases.

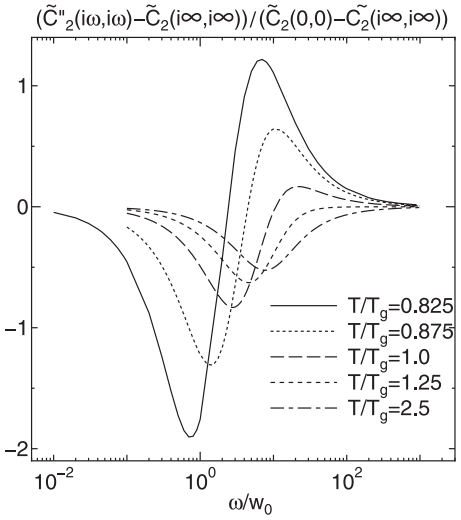

Figure 8. The imaginary part of the scaled second-order ac specific heat at temperatures $T/T_g = 0.825$, 0.875, 1.0, 1.25 and 2.5: as the temperature is decreased below the temperature $T_x/T_g = 1.25$, a local minimum decreases and a local maximum increases.

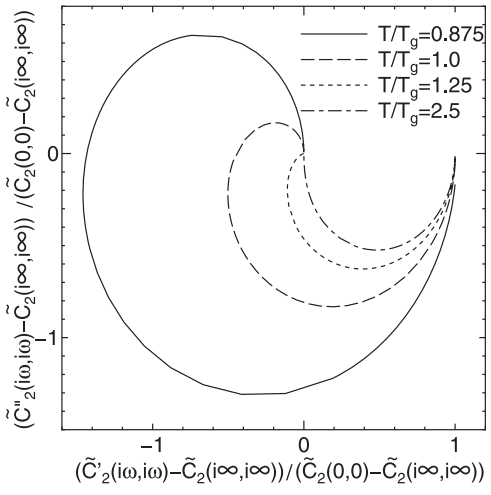

Figure 9. The Cole–Cole plot of the scaled second-order ac specific heat at temperatures $T/T_g = 0.875$, 1.0, 1.25 and 2.5: at a high temperature, the plots are semicircles. As the temperature is decreased, the plots deviate from semicircles.

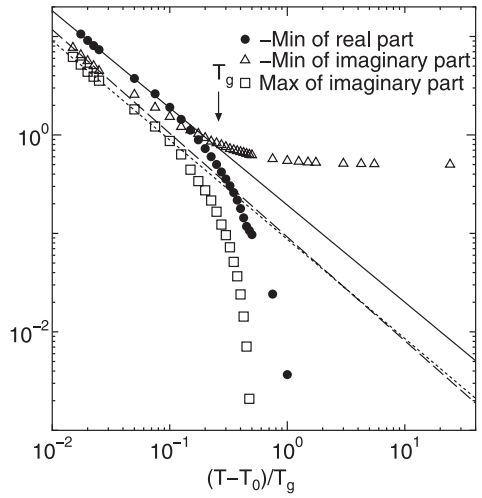

Figure 10. The temperature dependence of the extrema of the scaled second-order ac specific heat. The lines are fitted by power law functions in the low temperature region. Below T_g, the extrema obey the power law as $(T - T_0)^{-\nu}$. Above T_g, the temperature dependence of the extrema shows significant changes.

We analyzed the first- and second-order ac specific heats for a model glass former on the basis of the free energy landscape picture and showed characteristics of the ac specific heats.

A frequency ω_{peak} at a peak of the imaginary part of the first-order ac specific heat shifts to the low frequency region as the temperature is decreased below the glass temperature T_g and approaches zero at the Vogel–Fulcher temperature T_0. In the high temperature region above T_g, ω_{peak} becomes virtually independent of the temperature and approaches a constant value. The width of the peak becomes larger than that of the Debye relaxation type below T_g due to the distribution of the eigenvalue of the transition rate matrix λ and diverges at T_0. The statistics of λ such as $\langle\lambda\rangle$, $\langle\lambda^2\rangle$, and $\langle\lambda^{-1}\rangle$ can be obtained from the frequency dependence of the first-order ac specific heat, and these quantities show deviation from the Debye-type relaxation below T_g.

The scaled second-order ac specific heats have extrema, which obey the power law as $(T - T_0)^{\nu}$ below T_g. Above T_g, the temperature dependence of the extrema changes. The local minimum of the real part and the local maximum of the imaginary part vanish and the local minimum of the imaginary part approaches a constant value near the crossover temperature T_x.

The characteristics of the transition rate among basins reflect the frequency dependence of the first- and second-order ac specific heats. This means that the glass transition

point T_g, the Vogel–Fulcher temperature T_0 and the crossover temperature T_x can be determined from the first- and second-order ac specific heats. It is interesting to note that we can determine T_0, which is measured by the mechanical properties such as shear viscosity and diffusion coefficient, from the thermodynamic properties as the first- and second-order energy responses. We hope that the second-order ac specific heat will be measured for glass forming materials in experiment.

The framework of calculating the response to the external field with the free energy landscape picture is not limited in the energy response and can be also applied to other physical responses. For example, we can obtain the polarization response to the magnetic field when the distribution of the dipole moments at the basin is defined.

The main issue in calculating the physical response in the real system is how the basin is defined with the microscopic theories. We have considered that the free energy landscape obtained by the density functional theory can be used to define the basin [5] since the basin is defined as the local valley of the density functional. We expect that the free energy landscape picture will be evolved into microscopic theories in the future.

Acknowledgments

We would like to thank Professors Y Saruyama, O Yamamuro and A Yoshimori for useful discussions on this study. This work was supported in part by a Grant-in-Aid for Scientific Research from the Ministry of Education, Culture, Sports, Science and Technology.

Appendix

The ac specific heat can be measured from the temperature fluctuation when the energy is oscillated as heat flow. The ac specific heat is equal to the inverse of the coefficient of the temperature fluctuation with respect to the energy oscillation. Similar behavior is obtained in the second-order ac specific heat.

The temperature fluctuation $\Delta T(t)$ is assumed to follow the following equation:

$$\Delta T(t) = \int_0^t \mathrm{d}t_1 D_1(t-t_1)\Delta E(t_1) + \int_0^t \mathrm{d}t_1 \int_0^t \mathrm{d}t_2 D_2(t-t_1, t-t_2) \times \Delta E(t_1)\Delta E(t_2) + \mathrm{O}(\Delta E^3). \quad (41)$$

Here D_1 and D_2 are the retardation effects of first- and second-order energy perturbation $\Delta E(t)$, respectively. The Fourier transform of $\Delta T(t)$, $\Delta T(\omega)$, is expressed as follows.

$$\Delta T(\omega) = \tilde{D}_1(\mathrm{i}\omega)\Delta E(\omega) + \int \mathrm{d}\omega_1 \tilde{D}_2(\mathrm{i}\omega_1, \mathrm{i}\omega - \mathrm{i}\omega_1) \times \Delta E(\omega_1)\Delta E(\omega - \omega_1) \quad (42)$$

where

$$\tilde{D}_1(p) = \int_0^\infty \mathrm{d}t\, \mathrm{e}^{-pt} D_1(t) \quad (43)$$

$$\tilde{D}_2(p_1, p_2) = \int_0^\infty \mathrm{d}t_1 \int_0^\infty \mathrm{d}t_2\, \mathrm{e}^{-p_1 t_1}\mathrm{e}^{-p_2 t_2} D_2(t_1, t_2). \quad (44)$$

A similar expression of the expansion $\Delta E(\omega)$ with respect to $\Delta T(\omega)$ is shown in equation (4). The next relations are obtained with substituting equation (4) to (42).

$$\tilde{C}_1(\mathrm{i}\omega) = \frac{1}{\tilde{D}_1(\mathrm{i}\omega)} \quad (45)$$

$$\tilde{C}_2(\mathrm{i}\omega_1, \mathrm{i}\omega_2) = -\frac{\tilde{D}_2(\mathrm{i}\omega_1, \mathrm{i}\omega_2)}{\tilde{D}_1(\mathrm{i}\omega_1)\tilde{D}_1(\mathrm{i}\omega_2)\tilde{D}_1(\mathrm{i}\omega_1 + \mathrm{i}\omega_2)}. \quad (46)$$

Thus the second-order ac specific heat can be measured from the observation of the temperature fluctuation with respect to the energy oscillation.

References

[1] Gibson G E and Giauque W F 1923 *J. Am. Chem. Soc.* **45** 93
[2] Mézard M and Parisi G 1999 *J. Chem. Phys.* **111** 1076–95
[3] Goldstein M 1969 *J. Chem. Phys.* **51** 3728–39
[4] Sciortino F 2005 *J. Stat. Mech.* P5015
[5] Odagaki T, Yoshidome T, Koyama A and Yoshimori A 2006 *J. Non-Cryst. Solids* **352** 4843–6
[6] Odagaki T and Ekimoto T 2007 *J. Non-Cryst. Solids* **353** 3928–31
[7] Odagaki T and Hiwatari Y 1990 *Phys. Rev.* A **41** 929–37
[8] Odagaki T, Yoshidome T, Tao T and Yoshimori A 2002 *J. Chem. Phys.* **117** 10151–5
[9] Odagaki T, Tao T and Yoshimori A 2002 *J. Non-Cryst. Solids* **307–310** 407–11
[10] Tao T, Yoshimori A and Odagaki T 2002 *Phys. Rev.* E **66** 041103
[11] Tao T, Odagaki T and Yoshimori A 2005 *J. Chem. Phys.* **122** 044505
[12] Chakrabarti D and Bagchi B 2004 *J. Chem. Phys.* **120** 11678–85
[13] Chakrabarti D and Bagchi B 2005 *J. Chem. Phys.* **122** 014501
[14] Tagawa F and Odagaki T 2006 *J. Phys. Soc. Japan* **75** 124003
[15] Yamamuro O, Tsukushi I, Lindqvist A, Takahara S, Ishikawa M and Matsuo T 1998 *J. Phys. Chem.* B **102** 1605–9
[16] Birge N O and Nagel S R 1985 *Phys. Rev. Lett.* **54** 2674–7
[17] Christensen T 1985 *J. Physique Coll.* **46** C8 635
[18] Nielsen J K and Dyre J C 1996 *Phys. Rev.* B **54** 15754–61
[19] Odagaki T 1995 *Phys. Rev. Lett.* **75** 3701–4
Odagaki T 1997 *Prog. Theor. Phys. Suppl.* **126** 9–12